Research Square

Preprints are preliminary reports that have not undergone peer review.
They should not be considered conclusive, used to inform clinical practice,
or referenced by the media as validated information.

Characterization of inter-antibody variability in clinical pharmacokinetics of monoclonal antibodies using low-dimensional neural ordinary differential equations (NODE)

Devam A. Desai

devamdesai@ufl.edu

University of Florida

Rodrigo Cristofoletti

University of Florida

Article

Keywords:

Posted Date: November 9th, 2026

DOI: https://doi.org/10.21203/rs.3.rs-11055972/v1

License: This work is licensed under a Creative Commons Attribution 4.0 International License.
Read Full License

Additional Declarations: No competing interests reported.

Characterization of inter-antibody variability in clinical pharmacokinetics of monoclonal antibodies using low-dimensional neural ordinary differential equations (NODE)

Devam A. Desai[1] and Rodrigo Cristofoletti[1]

[1] Department of Pharmaceutics, College of Pharmacy, University of Florida, USA

Devam A. Desai

ORCID: https://orcid.org/0009-0006-8880-8718

Rodrigo Cristofoletti

ORCID: https://orcid.org/0000-0003-2619-0343

Corresponding Author: Rodrigo Cristofoletti

Corresponding Author email: rcristofoletti@ufl.edu

Funding Declaration: No funding was received for this work.

Conflict of Interest: The authors declared no competing interests for this work

Abstract:

Monoclonal antibodies (mAbs) exhibit high inter-antibody variability in clinical pharmacokinetics (PK), influenced by both molecular and physiological factors. Traditional models, including PBPK and TMDD frameworks, provide mechanistic detail but can be computationally intensive and limited in their ability to generalize across diverse antibodies. Neural ordinary differential equations (NODEs) represent a flexible, low-dimensional alternative that combines mechanistic interpretability with machine learning adaptability. This study aimed to apply NODE-based modeling to characterize inter-antibody PK variability and assess predictive generalizability across a large set of clinical mAbs. A comprehensive dataset of 36 mAbs (21 approved and 15 investigational at the time of the source publication), comprising 143 dose-route concentration-time profiles, was assembled, and two NODE-based frameworks were developed: i) NODE-2CMT, a two-compartment disposition model in which a single-hidden-unit neural network replaces an explicit Michaelis-Menten/target-mediated elimination term, and ii) NODE-mPBPK, a second-generation two-pore minimal PBPK model in which plasma elimination is represented entirely by the same network. Both models were estimated in Monolix on a training set of 31 antibodies (128 profiles, 1,259 observations) and evaluated using goodness-of-fit diagnostics, prediction-corrected visual predictive checks, and an antibody-level train/test split, with five antibodies (15 profiles, 164 observations) withheld from estimation entirely. Both frameworks described

the training data closely, the NODE-2CMT model giving the lower objective function value (ΔOFV = 553.7 at an equal number of estimated parameters). On the held-out antibodies, and without re-estimation of any population parameter, predictive accuracy was comparable and acceptable for both models (NODE-2CMT: absolute average fold error [AAFE] 1.40, average fold error [AFE] 1.13, 89% of predictions within 2-fold; NODE-mPBPK: AAFE 1.39, AFE 1.05, 92% within 2-fold), so the better in-sample fit did not translate into better out-of-sample prediction. Direct interrogation of the fitted networks showed that, across the observed concentration range, both learned elimination functions were effectively linear, implying apparent plasma clearances of 6.78 mL/h (NODE-2CMT, additional to an explicit linear clearance of 3.04 mL/h) and 11.2 mL/h (NODE-mPBPK); no saturable elimination component was identified in this dataset. Low-dimensional NODEs can be embedded in mechanistic antibody PK models, estimated jointly with between-antibody random effects, and applied to antibodies that did not contribute to estimation. They therefore hold promise for cross-molecule learning and for translational PK prediction in therapeutic antibody development, provided the learned term is reported and interpreted as a data-driven elimination function rather than as evidence of a specific disposition mechanism.

Introduction

Monoclonal antibodies (mAbs) constitute one of the fastest-growing classes of therapeutics, and their pharmacokinetics (PK) differ fundamentally from those of small molecules. Disposition is dominated by convective and lymphatic distribution into tissues, protection from catabolism through neonatal Fc receptor (FcRn) recycling, and, for many antibodies, binding to a pharmacological target [1, 2]. The resulting concentration–time profiles typically combine a slow, FcRn-mediated linear elimination pathway with a saturable, target-dependent component that becomes most apparent at low concentrations[3, 4]. Quantitative characterization of these processes is central to dose selection, to the design of first-in-human studies, and to the translation of preclinical data to the clinic.

The target-mediated drug disposition (TMDD) framework provides a mechanistic account of nonlinear antibody elimination by explicitly representing drug–target binding, internalization, and turnover[5]. Because the full TMDD model is rarely identifiable from typical clinical data, reduced forms such as the quasi-equilibrium and quasi-steady-state approximations are widely used[6, 7]. These approximations remain valuable, but they require assumptions about target expression, affinity, and turnover that are frequently unavailable early in development, and the associated parameters are often poorly determined when only plasma concentrations are observed.

Physiologically-based pharmacokinetic (PBPK) models offer a complementary, mechanism-rich description in which antibody distribution is governed by plasma and lymph flows and by size-dependent vascular reflection[8, 9]. Minimal PBPK formulations, in particular the second-generation two-pore model of Cao and Jusko, reduce the full

platform model to a small number of lumped tissue compartments while retaining a physiological interpretation of extravasation and lymphatic return[8-11]. Such models have become a standard tool in antibody development [12], yet they still embed prespecified elimination terms and rely on fixed physiological assumptions that may not capture molecule-specific nonlinear behavior[13].

A further challenge is that disposition varies considerably from one antibody to another, even within a single therapeutic area. Population PBPK analyses across large collections of antibodies have shown that much of this inter-antibody variability can be attributed to differences in target engagement and tissue distribution rather than to FcRn-mediated catabolism alone[13]. Characterizing this variability in a way that does not require a fully specified target system for every molecule would be valuable for cross-molecule learning and for prediction in data-sparse settings.

Neural ordinary differential equations (NODEs) provide a route to this goal by representing part of the system dynamics with a neural network whose parameters are estimated from data[14]. When a neural network is embedded within a partly mechanistic differential equation — a construction also described under the umbrella of universal differential equations and scientific machine learning — the known structure is retained while the unknown or poorly characterized terms are learned[15]. Neural networks are universal function approximators[16], and NODE-based approaches have been applied to pharmacokinetic problems including the prediction of new dosing regimens and the modeling of time-series concentration data[17-19]. A practical obstacle for population analysis is that high-capacity networks introduce many non-identifiable parameters that are incompatible with nonlinear mixed-effects estimation. Bräm and colleagues

addressed this by introducing low-dimensional NODEs, in which a deliberately small network is embedded in a compartmental model and estimated together with random effects in standard population software such as Monolix and NONMEM[20, 21]. This low-dimensional design preserves estimability while allowing the data to inform the shape of the nonlinear elimination.

In this work we apply the low-dimensional NODE concept to the clinical PK of mAbs across many molecules. We develop two hybrid models that differ in their mechanistic backbone: NODE-2CMT, which embeds a single-neuron network in a two-compartment disposition model at the structural position that an explicit Michaelis–Menten or TMDD elimination term would occupy, without imposing the saturable kinetics such a term would carry, and NODE-mPBPK, which embeds the same network within a second-generation two-pore minimal PBPK structure. Both models are fitted to a harmonized clinical dataset spanning intravenous (IV) and subcutaneous (SC) administration, with antibody-to-antibody differences represented as inter-individual variability. We evaluate the two frameworks using goodness-of-fit diagnostics, prediction-corrected visual predictive checks, and an antibody-level train/test split in which five antibodies were withheld from estimation entirely, and we compare their parameter estimates, statistical fit, learned elimination functions, and out-of-sample predictive accuracy.

Methods

Clinical monoclonal antibody pharmacokinetic database

A clinical pharmacokinetic (PK) dataset for approved and investigational monoclonal antibodies (mAbs) was assembled from publicly available sources [2-4, 22-54], including peer-reviewed clinical pharmacology publications and regulatory review documents when available. The database-building strategy was adapted from the inter-antibody PK workflow reported by Kumar et al.[13], in which published mAb concentration-time profiles were identified through literature and regulatory-source searches and digitized when numerical datasets were not available[13]. Published PK profile was prioritized when they provided sufficient concentration-time information after intravenous (IV) and/ or subcutaneous (SC) administration to support model-based characterization of disposition and absorption. Consistent with prior mAb PK database development, profiles consisting only of trough concentrations were not included because sparse trough-only datasets do not adequately define the absorption, distribution, or terminal disposition phases[13]. The data from the first dosing cycle of multiple dosing study was utilized in the analysis, all the PK profiles were digitized using Webplot digitizer[55] to build the dataset of 36 mAbs listed in Table 1. Of these, 21 were approved and 15 were investigational at the time of the source publication; together they contributed 143 dose-route concentration-time profiles and 1,423 concentration observations. Trastuzumab is not part of the present dataset.

Model Development

Two hybrid mechanistic-neural ordinary differential equation models were developed to characterize inter-antibody variability in clinical mAb PK: a two-compartment NODE model (NODE-2CMT; designated NODE-2CMT in earlier drafts of this work) and a NODE-minimal physiologically based pharmacokinetic model (NODE-mPBPK). The NODE-2CMT model as shown in Figure 1A incorporated classical compartmental PK terms for systemic distribution and elimination together with a learned elimination component occupying the structural position of a Michaelis-Menten or target-mediated term. The NODE-2CMT model described mAb disposition using a central compartment, peripheral distribution, linear clearance, SC absorption when applicable, and an additional learned elimination flux. The mechanistic component included linear clearance from the central compartment and intercompartmental exchange between central and peripheral compartment. A learned elimination flux was incorporated at the same position in the central-compartment mass balance that a Michaelis–Menten or target-mediated term would occupy[5, 56]. It is important to be explicit about what this term is and is not. The learned flux is a single-hidden-unit rectified-linear-unit (ReLU) function of the central amount and is therefore continuous and piecewise-linear in its input. It is not a Michaelis–Menten expression, and it does not represent drug-target binding, internalization, or target turnover. It carries none of the structural constraints of saturable elimination: it is not bounded above, it does not approach a maximum flux, and it can reproduce saturation-like curvature only to the extent that a single change of slope can do so. The model is therefore designated NODE-2CMT rather than NODE-MM-TMDD, and the embedded term is referred to throughout as a learned elimination function motivated by, but not equivalent to, Michaelis–Menten/TMDD behaviour. The

NODE-mPBPK as shown in Figure 1B was developed as a reduced-order physiologically informed model representing antibody distribution and elimination using minimal PBPK concepts, including tissue distribution processes and reflection-coefficient terms for tight and leaky tissues[8, 9]. Minimal PBPK models have been used to describe mAb plasma PK while retaining physiologic interpretation of tissue distribution and lymphatic return processes. In the present model, the mPBPK framework included distribution processes governed by physiologically interpretable reflection-coefficient parameters representing drug transport into tight and leaky tissue spaces[8, 9]. A neural network term was incorporated to capture inter-antibody variability in elimination of mAbs.

The models were constructed as low-dimensional NODE pharmacometrics models, in which pre-specified mechanistic equations were retained for known PK processes and neural network functions were embedded within ordinary differential equation systems to represent less well-characterized antibody-dependent processes[20, 21]. This hybrid structure was selected to preserve mechanistic interpretability while allowing flexible characterization of inter-antibody differences in clearance. This approach is consistent with the scientific machine-learning framework in which mechanistic model components describe known biological processes and neural network terms are used to learn residual or incompletely specified dynamics[14, 20].

Neural ordinary differential equation structure

Neural network components were implemented as low-dimensional feed-forward neural networks embedded directly into the differential equations mentioned in Supplementary Information (Appendix S1). Neural ordinary differential equations parameterize the

derivative of a system state using a neural network, allowing continuous-time dynamics to be learned from longitudinal data[14]. Low-dimensional NODEs extend this concept for pharmacometrics applications by using compact neural networks without high-dimensional latent states, thereby improving compatibility with standard pharmacometrics software and nonlinear mixed-effects estimation.

For a model input x, the neural network component was represented as:

$$f_{NN}(x) = i = \sum_{i=1}^{n_H} w_{2,i}\, max(0, w_{1,i}x + b_{1,i}) + b_2$$

Where n_H is the number of hidden units, $w_{1,i}$ and $b_{1,i}$ are the input weight and bias for hidden unit i, $w_{2,i}$ is the output weight, b_2 is the output bias, and $max(0,\cdot)$ denotes the rectified linear unit activation function. This structure follows the low-dimensional NODE implementation described for Monolix[20, 21]. State-dependent neural terms were used to represent antibody-dependent elimination processes.

Inter- Antibody Variability and Residual Error

Inter-antibody variability was modeled using nonlinear mixed-effect methods. Each antibody or antibody-dose-route profile was treated analogously to an individual modeling unit, an approach similar to prior inter-antibody population PBPK modeling in which each antibody was treated as an individual to estimate population and antibody-specific parameters Because the modelling unit is a published dose-route profile rather than a subject, the resulting random effects should not be read as inter-antibody variability alone. A single antibody may contribute several profiles that differ in route, dose level, study population, sampling schedule, bioanalytical method, and digitization

error, and all of these sources of difference are absorbed into the same random-effect terms. The variance components reported here therefore represent combined between-profile variability, confounding inter-antibody, inter-study, inter-route, and inter-dose contributions, and the term "inter-antibody variability" is used throughout in this broader sense.[13]. For positive-valued mechanistic PK parameters, antibody-specific parameter values were assumed to follow a log-normal distribution:

$$P_j = P_{pop}\exp(\eta_{P,j})$$

Where $P_j$is the antibody-specific parameter value for antibody j, Ppop is the typical population value, and np,j is a normally distributed random effect with mean zero and variance. For neural network weights and bias parameters, normal or fixed-effect parameterization was used as appropriate because neural network parameters are not constrained to be positive and may take either positive or negative values[21]. Random effects were retained when supported by stable estimation, acceptable precision, diagnostic improvement, and biological or model-based plausibility. Residual unexplained variability was described using a combined additive and proportional error model:

$$Y_{ij} = C_{ij} + \epsilon_{add,ij} + C_{ij\epsilon_{prop},ij}$$

Where Y_{ij} is the observed concentration for observation and antibody j, C_{ij} is the model-predicted concentration, E and E are normally distributed additive and proportional residual error terms, respectively. A combined residual error model was selected because clinical mAb PK data were obtained from multiple published sources and therefore may contain both concentration-independent and concentration-dependent

residual variability[13]. Models were implemented in Monolix 2024R1[57] and estimated using the stochastic approximation expectation-maximization algorithm. SAEM-based nonlinear mixed-effects estimation and Fisher information matrix-based standard error calculation have been used previously for inter-antibody population PK modeling in Monolix. The NODE model-building working followed the low-dimensional NODE-PMX implementation described by Bräm et al. [21] Briefly structural models were first fit without inter-antibody random effects to stabilize estimation of the mechanistic and neural fixed effects. The resulting parameter estimates were then used as initial estimates for the final nonlinear mixed effects model with inter-antibody variability[21]. Neural network weights and biases were initialized to avoid inactive ReLU units over the observed or expected range of model inputs, consistent with recommendations for low-dimensional NODE implementation in pharmacometric software[20, 21]. For time-dependent neural network terms, input weights were constrained to avoid unbounded increases at late times[21]. Final parameter precision was summarized using relative standard error (%RSE), and standard errors were obtained from the Fisher information matrix. Diagnostic evaluation included observed-versus-population-predicted and observed-versus-individual-predicted concentration plots, residual diagnostic plots, and visual predictive checks. These diagnostics were used to evaluate whether the final models adequately described the central tendency and variability of the observed concentration–time profiles across antibodies and routes of administration. Model evaluation was extended beyond these in-sample diagnostics by the antibody-level train/test analysis described in the following section.

Antibody-level train/test split and out-of-sample evaluation

To assess whether the learned elimination functions generalize to antibodies that did not contribute to estimation, the dataset was partitioned at the antibody level before any model fitting. Five antibodies — daclizumab, fulranumab, nivolumab, obiltoxaximab and raxibacumab — were withheld as a test set, contributing 15 dose-route profiles and 164 concentration observations. These molecules were selected to span the behaviours present in the dataset: two contributed both intravenous and subcutaneous data (daclizumab, fulranumab), one contributed dose-ranging intravenous data on a mg/kg basis (nivolumab), and two contributed single high-dose intravenous profiles at the upper end of the observed exposure range (obiltoxaximab, raxibacumab). The remaining 31 antibodies, comprising 128 dose-route profiles and 1,259 observations, constituted the training set. All population parameters, random-effect variances, and residual error parameters reported in this work were estimated from the training set alone; the test antibodies contributed nothing to estimation.

Test antibodies were then evaluated without re-estimation of any population parameter. Because the antibody-specific random effects of a molecule not seen during estimation are by definition unknown, test-set predictions were generated by fixing the population parameters, random-effect variances, and residual error model to the training estimates and obtaining antibody-specific random effects as empirical Bayes estimates conditional on the observed test data. This corresponds to the practical situation in which a limited amount of clinical PK data becomes available for a new antibody and an established platform model is used to describe it. It does not correspond to fully a priori prediction from molecular or target properties alone, which the present models cannot perform because they contain no molecular descriptors; that limitation is discussed below.

Predictive performance on the test set was summarized using the average fold error (AFE), the absolute average fold error (AAFE), and the proportion of predicted concentrations falling within 2-fold of the corresponding observation. AFE was calculated as 10 raised to the mean of log10(Cpred/Cobs) across all paired observations, and AAFE as 10 raised to the mean of the absolute value of log10(Cpred/Cobs), where Cpred and Cobs denote the predicted and observed concentrations. AFE quantifies systematic bias, with values above and below 1 indicating over- and under-prediction respectively, while AAFE quantifies overall precision, with a value of 1 indicating exact agreement. A 2-fold criterion was adopted because it is the accuracy conventionally regarded as acceptable for mechanistic and platform PK model predictions of monoclonal antibody exposure.

Results

NODE-2CMT model

The NODE-2CMT model described the clinical concentration–time data of the 31 training antibodies across both routes of administration (Figure 2). Individual predictions closely tracked the observed profiles over several orders of magnitude in concentration, reproducing the multiphasic decline characteristic of intravenous antibody disposition as well as the absorption-limited rise and fall seen after subcutaneous administration. Within antibodies that contributed dose-ranging data, the model captured the separation between dose levels. Fit quality was most consistent for antibodies with densely sampled, multi-dose profiles and was necessarily more uncertain for antibodies represented by sparse or single-dose data.

The estimated typical linear clearance (CL) was 3.04 mL/h with good precision (%RSE = 8.82). The central volume of distribution (Vc) was estimated as 3,490 mL (%RSE = 5.57), and the peripheral volume of distribution (Vp) was estimated as 2,560 mL (%RSE = 2.45). Intercompartmental clearance (Q) was estimated as 21.2 mL/h (%RSE = 4.89),

and the subcutaneous absorption-rate constant (ka) was estimated as 0.0167 h^-1 (%RSE = 4.61). All four neural-network parameters were estimated with acceptable precision: W11 = 0.00615 (%RSE = 12.8), b11 = 0.0295 (%RSE = 33.0), Wc21 = 0.316 (%RSE = 16.5), and bc21 = 0.0243 (%RSE = 30.5). Between-antibody variability was retained on central volume of distribution and on the network output weight Wc21. The estimated random-effect standard deviations were 0.608 for Vc (%RSE = 6.44) and 0.873 for Wc21 (%RSE = 7.01), with low eta-shrinkage of 2.0% and 5.7% respectively, as described in Table 2. Residual variability was described by a combined error model with additive and proportional components of 0.0365 µg/mL (%RSE = 10.0) and 0.154 (%RSE = 2.40). Diagnostic plots shown in Figure S1 (A and B) indicate good agreement between observed and individual predicted concentrations across antibodies, with no major systematic bias across the observed concentration range. The prediction-corrected visual predictive check showed that the final model captured the central tendency of the observed data and reproduced the overall variability in the concentration–time profiles.

NODE-mPBPK model

The NODE-mPBPK model also described the clinical concentration–time profiles of the 31 training antibodies, as shown in Figure 3. The model included reduced-order physiologic distribution parameters, subcutaneous absorption, and network parameters representing antibody-dependent elimination. As shown in Table 2, the estimated vascular reflection coefficient for tight tissues (σ_1) was 0.914 (%RSE = 1.63), and that for leaky tissues (σ_2) was 0.729 (%RSE = 2.20); both values are close to those reported for immunoglobulin G in the second-generation minimal PBPK model. The

subcutaneous absorption-rate constant (ka) was estimated as 0.00735 h^-1 (%RSE = 25.2). The network parameters were estimated as W11 = 56.4 (%RSE = 10.1), b11 = -3.15 (%RSE = 27.9), Wc21 = 0.199 (%RSE = 11.2), and bc21 = 0.169 (%RSE = 40.7); precision was therefore acceptable for all four parameters in the present fit, with the output bias bc21 the least well determined. Between-antibody variability was retained on the two reflection coefficients, on the absorption-rate constant, and on the network output weight, with estimated standard deviations of 0.0934 (σ_1), 0.168 (σ_2), 1.12 (ka), and 0.116 (Wc21). Eta-shrinkage was low for Wc21 (1.9%) and moderate for σ_2 (19.6%), but was appreciable for σ_1 (35.9%) and high for ka (58%); the latter reflects the smaller number of profiles contributing subcutaneous data, and individual ka estimates should be interpreted with corresponding caution. Residual variability comprised additive and proportional components of 0.0290 µg/mL (%RSE = 12.1) and 0.164 (%RSE = 2.44). Diagnostic plots shown in Figure S2 (A and B) demonstrated that the model captured the overall concentration–time profiles across antibodies, including the range of IV and SC profiles, and the prediction-corrected visual predictive check showed that the model described the central tendency and dispersion of the observed data.

Characterization of the learned elimination functions

Because individual network weights carry no direct interpretation, the fitted networks were interrogated as functions: the learned elimination flux fNN was evaluated across the full range of network inputs actually visited by the training data, with the realized input distribution shown as a rug beneath each curve (Figure S3). In both models the learned function was, over that range, indistinguishable from a straight line.

In the NODE-2CMT model the hidden-unit input bias was positive (b11 = 0.0295) while the network input, the central amount, is non-negative. The ReLU unit was therefore active over the whole of its domain, and the learned flux reduced exactly to the affine function $fNN = Wc21 \cdot W11 \cdot Ap + (Wc21 \cdot b11 + bc21) = 1.94 \times 10^{-3} \cdot Ap + 0.0336$, with no breakpoint anywhere in the observed or extrapolated range. Expressed on a concentration basis this corresponds to $fNN \approx 6.78 \cdot Cp + 0.0336$, that is, an apparent additional plasma clearance of 6.78 mL/h that does not vary with concentration. The fitted model is thus functionally a two-compartment model with first-order elimination, in which the total apparent clearance is the sum of the explicit linear clearance and the learned contribution, 3.04 + 6.78 = 9.82 mL/h, or 0.236 L/day.

In the NODE-mPBPK model the hidden-unit input bias was negative (b11 = -3.15), so the ReLU unit was inactive below a plasma concentration of -b11/W11 = 0.0559 µg/mL and active above it. The learned flux was therefore genuinely piecewise-linear, but the breakpoint lay at or below the lowest observed concentrations, so that across essentially the entire observed range the function was again linear, $fNN \approx 11.2 \cdot Cp - 0.458$. This corresponds to an apparent plasma clearance of 11.2 mL/h, or 0.269 L/day. Because plasma elimination in this structure is represented entirely by the network, this value is the model estimate of total apparent clearance rather than an increment to an explicit clearance term.

Two observations follow. First, both apparent clearances fall within the range reported for endogenous and therapeutic immunoglobulin G, so the networks recovered physiologically plausible elimination without being constrained to do so. Second, and more consequential for interpretation, neither network identified a saturable elimination

component in this dataset. The capacity to represent a change of slope was available in both models and was used in only one of them, at a concentration below the observed range. The learned terms should accordingly be read as data-driven, effectively linear elimination functions and not as evidence of target-mediated disposition. This is consistent with the composition of the dataset, which consists predominantly of mean profiles at or near clinically used dose levels, where any target-mediated pathway is frequently saturated and contributes comparatively little to the observed decline.

Prediction of antibodies withheld from estimation

Neither model saw daclizumab, fulranumab, nivolumab, obiltoxaximab or raxibacumab during estimation. Applying the training population parameters to these five antibodies gave comparable and acceptable accuracy for both frameworks across 164 held-out observations spanning approximately five orders of magnitude in concentration (Figure 4, Table 3). The NODE-2CMT model achieved an AAFE of 1.40 and an AFE of 1.13, with 89% of predictions falling within 2-fold of the observed concentration. The NODE-mPBPK model achieved an AAFE of 1.39 and an AFE of 1.05, with 92% within 2-fold. Precision was therefore essentially identical between the two models, while the NODE-mPBPK model showed less systematic bias; the AFE of 1.13 for the NODE-2CMT model indicates a modest overall tendency to over-predict.

Individual fits to the test antibodies are shown in Figure S4. Both models reproduced the intravenous and subcutaneous profiles of daclizumab, the dose-ranging intravenous and subcutaneous profiles of fulranumab, the mg/kg-based intravenous profiles of nivolumab, and the single high-dose intravenous profiles of obiltoxaximab and raxibacumab, including the approximately 1,000-fold difference in peak concentration between the

fulranumab and raxibacumab arms. The largest deviations for both models occurred at the lowest observed fulranumab concentrations, close to the assay lower limit of quantification, and at the earliest raxibacumab sampling time.

The ordering of the two models reversed between in-sample fit and out-of-sample prediction: the NODE-2CMT model gave the substantially lower objective function value on the training data but did not predict the held-out antibodies more accurately. Likelihood-based comparison of structurally different models on the estimation dataset therefore does not by itself establish which model will transfer to new molecules, and the two frameworks are better regarded as comparable in predictive performance on this dataset than as ranked.

Comparison of NODE-2CMT and NODE-mPBPK models

Both hybrid NODE frameworks recapitulated the observed clinical PK profiles of the 31 training antibodies. On the training data the NODE-2CMT model provided a lower objective function value and lower information criteria than the NODE-mPBPK model (OFV 5,433.36 versus 5,987.05; AIC 5,459.36 versus 6,013.05; BIC 5,496.44 versus 6,050.13), a difference of 553.69 points in objective function value at an equal number of estimated parameters (13 in each model), together with better goodness-of-fit (Figure S1 A and S2 A) and visual predictive check (Figure S1 B and S2 B) diagnostics. Because the two models differ structurally rather than hierarchically, these criteria should be interpreted as descriptive model-comparison metrics rather than as a formal statistical test, and, as described above, the advantage on the training data did not carry over to the antibodies withheld from estimation.

The NODE-2CMT model provided precise estimates for classical pharmacokinetic parameters, including clearance, distribution volumes, intercompartmental clearance, and absorption. The NODE-mPBPK model provided physiologically interpretable tissue-distribution parameters with high precision and, in the present analysis, acceptable precision for all four network parameters (Table 2). Overall, the results demonstrate that low-dimensional NODEs can be incorporated into mechanistic antibody PK models, estimated jointly with between-profile random effects across a diverse clinical mAb dataset, and applied to antibodies that did not contribute to estimation.

Discussion

We developed two low-dimensional neural ODE models for the clinical pharmacokinetics of monoclonal antibodies and showed that both can reproduce the disposition of a large and chemically diverse set of antibodies while characterizing inter-antibody variability. By embedding a deliberately small neural network within established mechanistic structures — a two-compartment disposition model and a second-generation minimal PBPK model — the approach learns the elimination contribution directly from concentration–time data rather than prescribing its functional form in advance. To our knowledge, this is among the first applications of the low-dimensional NODE concept to inter-antibody variability across a harmonized clinical mAb dataset of this breadth, and the first in which such a model is evaluated on antibodies withheld from estimation.

The two frameworks behaved in complementary ways. The NODE-2CMT model achieved a better statistical fit to the training data with fewer estimated structural parameters,

making it an attractive default when a parsimonious description is desired. The NODE-mPBPK model grounds the learned elimination within an explicitly physiological distribution structure and showed marginally less systematic bias on the held-out antibodies, which may make it preferable when mechanistic interpretation of tissue distribution is important or when extrapolation across dosing routes is required. Because out-of-sample accuracy was effectively equivalent, the choice between the two is better made on interpretive grounds than on fit statistics. The estimated reflection coefficients in the minimal-PBPK model were close to literature expectations for immunoglobulin G, indicating that embedding a neural network for elimination did not distort the physiological component of the model[8, 9].

The individual neural-network parameters were estimated with lower precision than the physiological parameters, although in the present analysis no network parameter exceeded a relative standard error of 41%. This is a known property of low-dimensional NODEs: the network is a flexible functional element rather than a set of mechanistic constants, and it is the learned function and its influence on the predicted profile — not the individual weights — that carry meaning[20, 21]. We do not, however, regard that argument as sufficient on its own. If the weights carry no interpretation, the burden of interpretation falls on the learned function, and the function should therefore be reported rather than merely asserted to be meaningful. We accordingly evaluated the learned elimination flux directly over its realized input domain (Figure S3) instead of relying on parameter precision alone, and that diagnostic proved informative in a way the weights were not: it showed that both networks collapsed onto effectively linear elimination, that the implied apparent clearances of 6.78 and 11.2 mL/h are physiologically plausible for

immunoglobulin G, and that the available capacity to represent saturation went essentially unused. We would encourage this diagnostic — plotting the learned term across the input values the data actually visit, together with a rug of those inputs — as routine practice whenever neural terms are embedded in pharmacometric models, since it converts an otherwise opaque component into an inspectable function and makes overclaiming considerably harder. It also follows that the network parameters are not comparable across the two models, because each network receives a differently scaled input and operates within a different structural context; only the resulting functions can meaningfully be compared.

Several limitations should be acknowledged, of which the most consequential concerns the modelling unit. The dataset was assembled from published, largely digitized mean concentration–time profiles, and each dose-route profile was treated as a separate estimation unit. A single antibody may contribute several such profiles — adalimumab, for example, contributes both intravenous and subcutaneous data, and several antibodies contribute multiple dose levels or more than one study population — and differences between those profiles may arise from route, dose, study design, patient population, sampling density, bioanalytical assay, or digitization error as readily as from any intrinsic property of the molecule. The random effects estimated here are therefore not pure inter-antibody variability: they represent between-profile variability that confounds inter-antibody, inter-study, inter-route, and inter-dose contributions, and the magnitude of the estimated omega values, together with the individual parameter estimates derived from them, should be interpreted with that confounding in mind. Disentangling these components would require either individual-subject data or a hierarchical structure with

antibody nested above study and route, neither of which the present data support. Relatedly, because the analysis describes representative rather than individual profiles, classical covariate analyses of patient factors were outside its scope.

Further limitations follow from the model structure and from the evaluation design. The models did not incorporate explicit target-system descriptors such as antigen expression or affinity, which are the mechanistic drivers of target-mediated elimination; the network instead summarizes their net effect on plasma disposition, and, as shown above, that net effect was linear in this dataset. The single-neuron architecture, chosen for identifiability, permits at most one change of slope and therefore constrains the class of elimination functions that can be represented; a network with additional hidden units, appropriately regularized, might resolve curvature that the present architecture cannot, and the absence of detected saturation should not be read as strong evidence that none exists. Because the network learns within the support of the observed data, predictions outside the observed concentration and dose ranges should be treated with caution, and the non-smoothness of the ReLU activation, while convenient, is a modeling choice that could be revisited. Finally, the out-of-sample evaluation rests on a single split of five antibodies, so the reported accuracy is itself uncertain; repeated splits or a full leave-one-antibody-out analysis would give a more stable estimate of generalization. Test-antibody random effects were obtained conditional on the observed test data, so the reported accuracy reflects the use of an established platform model to describe a new antibody for which some clinical PK data already exist, and not fully a priori prediction from molecular properties alone.

These results position low-dimensional NODEs as a complement to, rather than a replacement for, mechanistic modeling of antibody pharmacokinetics. They are most useful when the target system is incompletely characterized, when a common framework is needed to learn across many molecules, or when rapid, data-efficient description is required early in development. Natural extensions include informing the network input with molecular or target descriptors so that disposition can be predicted for new antibodies from their properties, the use of slightly larger but appropriately regularized networks, integration of the learned elimination within larger quantitative systems pharmacology models, and prospective evaluation in first-in-human prediction[58, 59]. The learned elimination functions could also serve as informative priors for subsequent mechanistic analyses.

Conclusion

Two low-dimensional neural ODE models — one built on a two-compartment structure and one on a second-generation minimal PBPK structure — described the clinical pharmacokinetics of 31 monoclonal antibodies and, without re-estimation of any population parameter, described the profiles of five further antibodies withheld from estimation with an absolute average fold error of approximately 1.4 and roughly 90% of predictions within 2-fold. The two-compartment NODE provided the more parsimonious and statistically favoured description of the training data, while the minimal-PBPK NODE showed marginally less bias on the held-out antibodies within an explicitly physiological framework; the two were otherwise equivalent in out-of-sample accuracy. Direct interrogation of the fitted networks showed that both learned elimination functions were effectively linear across the observed concentration range and implied physiologically

plausible apparent clearances, but provided no evidence of saturable elimination in this dataset. Low-dimensional NODEs are therefore a workable and inspectable means of learning elimination behaviour across many molecules within a mechanistic scaffold, provided the learned term is reported as a function and interpreted as such rather than as a mechanism.

Data Availability

The data analyzed in this study were derived from publicly available sources, including peer-reviewed publications and regulatory review documents, as cited in the article. Concentration–time data were digitized from the published pharmacokinetic profiles and compiled into a harmonized dataset for model development and evaluation. The compiled dataset generated and analyzed during the current study is available from the corresponding author upon reasonable request.

Figure 1. Structural schematics of the two low-dimensional neural ODE (NODE) models developed to characterize inter-antibody variability in monoclonal antibody pharmacokinetics. **(A) NODE-2CMT model.** A two-compartment disposition structure comprising a central compartment (C_c) and a peripheral compartment (C_p) connected by inter-compartmental clearance (Q), with linear clearance (CL) from the central compartment. A low-dimensional feed-forward neural network (dashed arrow) is embedded into the central-compartment elimination to capture concentration-

dependent, antibody-specific disposition at the structural position that an explicit Michaelis–Menten/target-mediated drug disposition term would occupy; the network does not impose saturable kinetics. Subcutaneous doses, when applicable, enter the central compartment through a first-order absorption process. **(B) NODE-mPBPK model.** A second-generation two-pore minimal physiologically-based structure in which antibody distributes from plasma into tight- and leaky-tissue compartments governed by vascular reflection coefficients σ_1 and σ_2 and lymph flows L_1 and L_2, drains into a common lymph compartment, and returns to plasma via total lymph flow L. Intravenous doses enter the plasma compartment directly (IV), and plasma elimination is represented entirely by the embedded neural network (dashed arrow). Physiological volumes and lymph flows were fixed to literature values for immunoglobulin G.

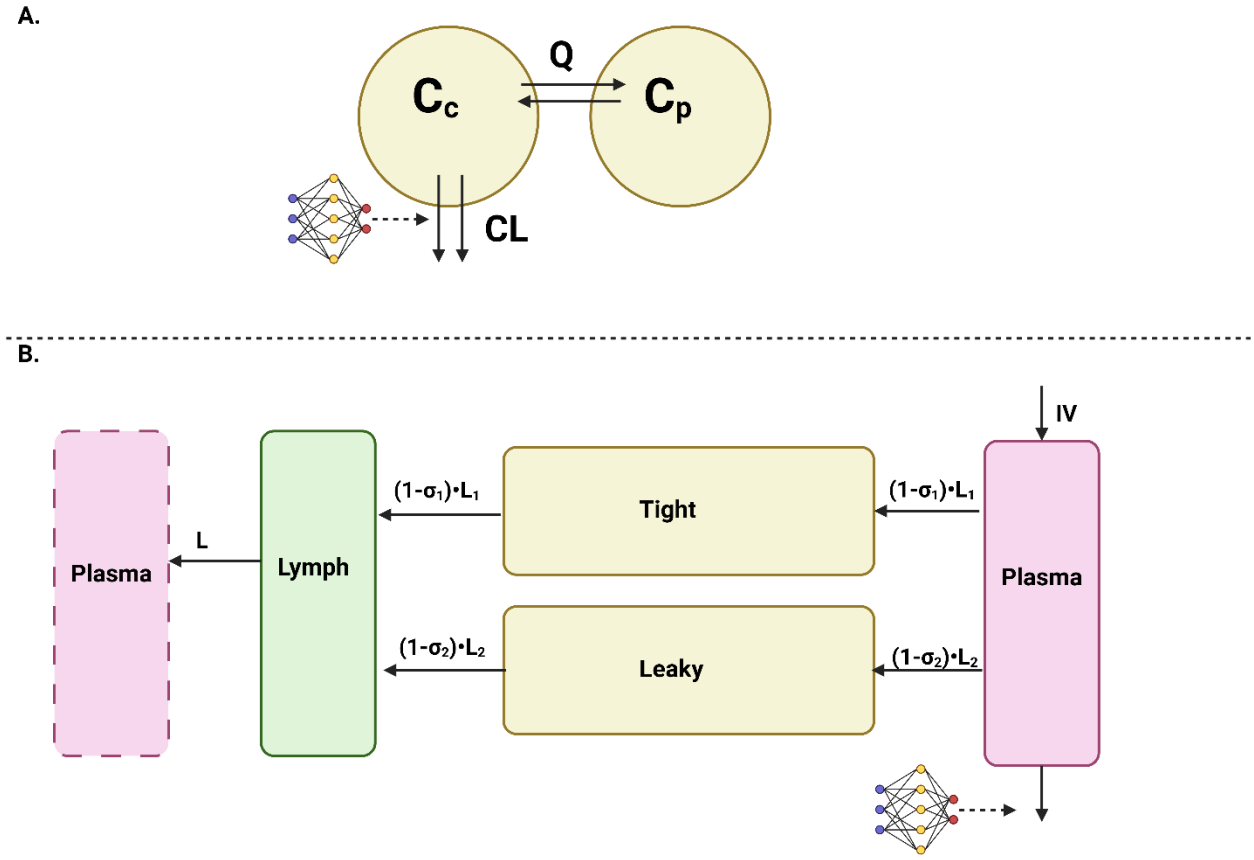
Figure 2. Individual NODE-2CMT model fits to clinical concentration–time data for the 31 antibodies of the training set. Each panel corresponds to a single antibody and route of administration (intravenous, IV; subcutaneous, SC), as indicated in the panel header. Points are observed concentrations and solid lines are individual model predictions; colors distinguish dose levels within each panel. Concentrations (μg/mL) are shown on a $\log_{10}$ scale against time (hours). Antibodies withheld as the test set are not shown here; their fits are given in Figure S4. The model reproduced both the multiphasic IV disposition and the absorption-limited SC profiles across antibodies spanning a wide range of clearances and exposures.

Figure 3. Individual NODE-mPBPK model fits to clinical concentration–time data for the 31 antibodies of the training set. Panels, symbols, lines, colors, and axes are as described for Figure 2; each panel shows a single antibody and route of administration

with observed concentrations (points) and individual model predictions (lines) on a semi-logarithmic scale. The minimal-PBPK NODE structure captured the central tendency and the between-profile dispersion of the observed profiles across both IV and SC administration.

Figure 4. Predicted versus observed concentrations for the five antibodies withheld from estimation. (A) NODE-2CMT model. (B) NODE-mPBPK model. Each point is a single observation from the held-out test set (n = 164 observations from daclizumab, fulranumab, nivolumab, obiltoxaximab and raxibacumab); colours distinguish antibodies. The solid line is the line of identity and the dashed lines delimit the 2-fold error envelope; both axes are log10-scaled. Summary statistics are given in each panel header: absolute average fold error (AAFE), average fold error (AFE), and the percentage of predictions falling within 2-fold of the corresponding observation. Population parameters, random-effect variances, and residual error parameters were estimated from the 31 training antibodies only and were not re-estimated for the test set; antibody-specific random effects for the test antibodies were obtained as empirical Bayes estimates conditional on the observed test data.

Figure 1.


A.
Q
C_c
C_p
CL
B.
IV
Plasma
L
Lymph
$(1-\sigma_1)\cdot L_1$
Tight
$(1-\sigma_1)\cdot L_1$
Plasma
$(1-\sigma_2)\cdot L_2$
Leaky
$(1-\sigma_2)\cdot L_2$

642

643

644

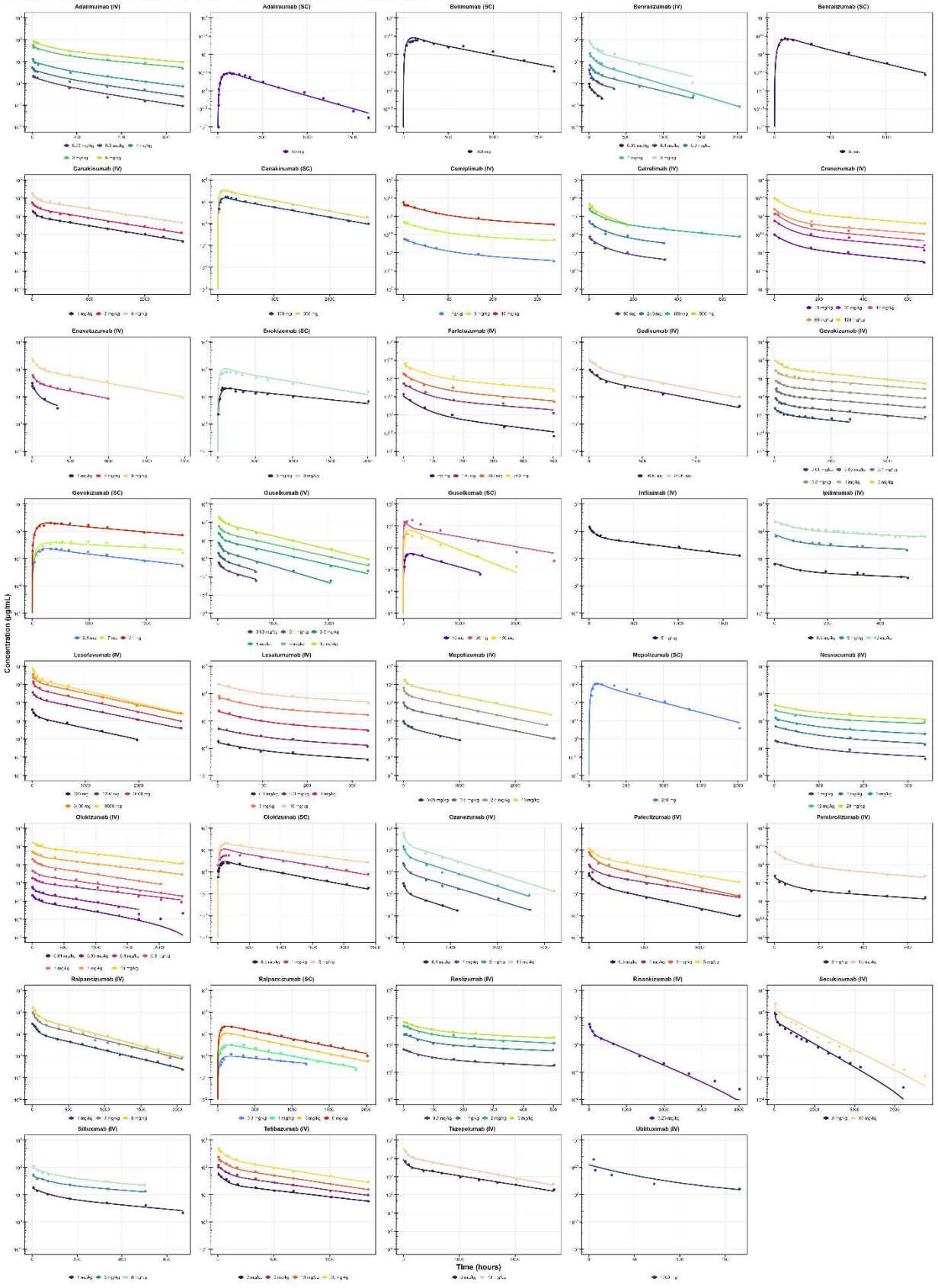
645

646

647

648 Figure 2.

649


NODE-2CMT model fittings overview across compounds and routes
Points = observed concentrations • lines = individual model fit (conditional mode). Y-axis log10, auto-scaled per panel (manual overrides via Y_OVERRIDES).
Adalimumab (IV)
Adalimumab (SC)
Belimumab (SC)
Benralizumab (IV)
Benralizumab (SC)
Canakinumab (IV)
Canakinumab (SC)
Camiplimab (IV)
Cetrelimab (IV)
Cronazumab (IV)
Enavaluzumab (IV)
Enokizumab (SC)
Farletuzumab (IV)
Gedivumab (IV)
Gevokizumab (IV)
Gevokizumab (SC)
Guselkumab (IV)
Guselkumab (SC)
Infliximab (IV)
Ipilimumab (IV)
Lesofavumab (IV)
Lexatumumab (IV)
Mepolizumab (IV)
Mepolizumab (SC)
Nesvacumab (IV)
Olokizumab (IV)
Olokizumab (SC)
Ozanezumab (IV)
Pateclizumab (IV)
Pembrolizumab (IV)
Ralpancizumab (IV)
Ralpancizumab (SC)
Reslizumab (IV)
Risankizumab (IV)
Secukinumab (IV)
Siltuximab (IV)
Telibazumab (IV)
Tezepelumab (IV)
Ublituximab (IV)
Concentration (ug/mL)
Time (hours)

651 Figure 3.

652

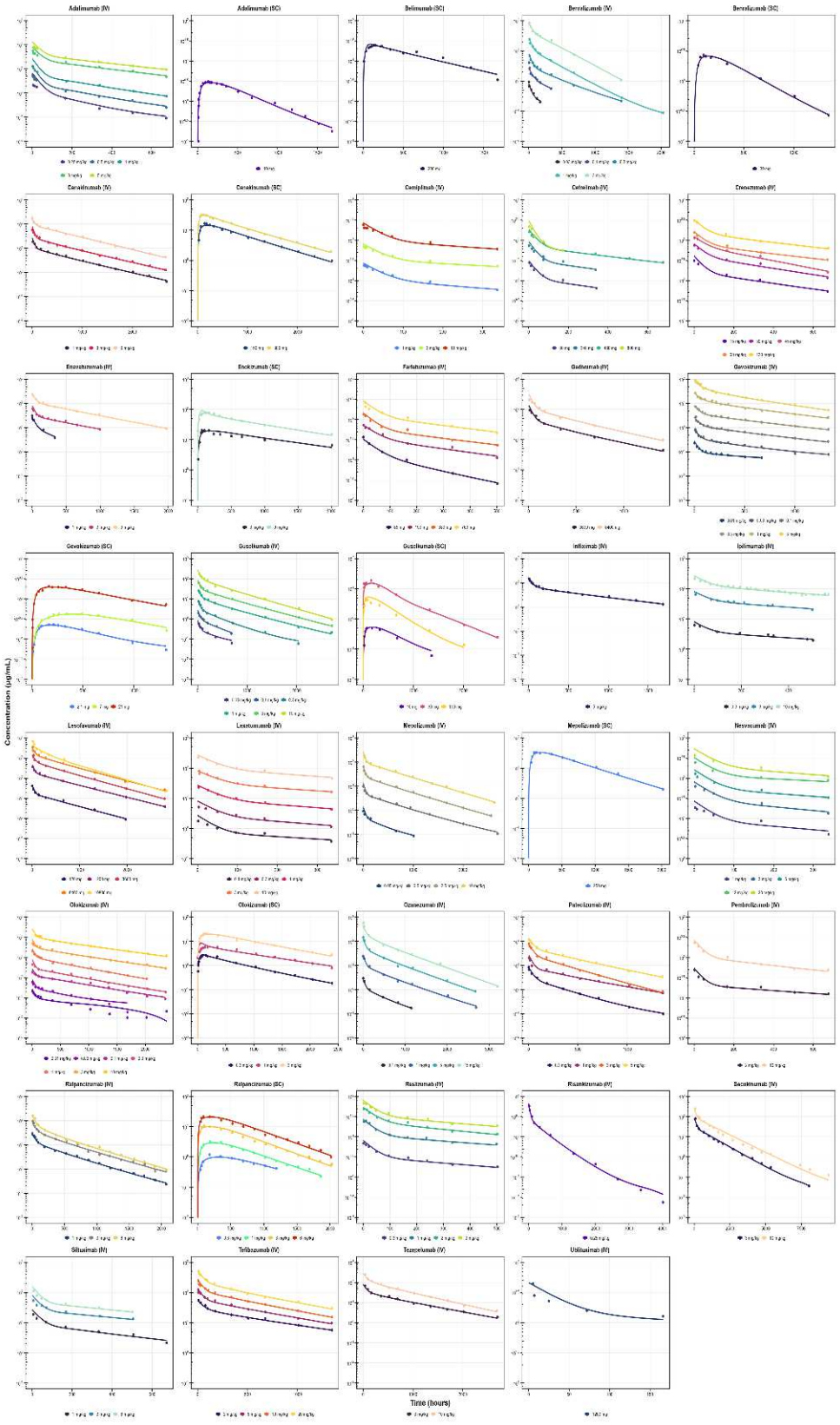

NN-mPBPK model fittings overview across compounds and routes
Points = observed concentrations • lines = individual-level fit (population mean). Y-axis log10, ratio-scales per panel (manual overrides via Y_OVERRIDES).
Adalimumab (IV)
Adalimumab (SC)
Belimumab (SC)
Berralizumab (IV)
Berralizumab (SC)
Canakinumab (IV)
Canakinumab (SC)
Certolizumab (IV)
Cetrelimab (IV)
Cravezumab (IV)
Enoxaparumab (IV)
Elotuzumab (SC)
Fanlatuzumab (IV)
Gadimumab (IV)
Gevokizumab (IV)
Gevokizumab (SC)
Guselkumab (IV)
Guselkumab (SC)
Infliximab (IV)
Ipilimumab (IV)
Lesofavumab (IV)
Lexatumumab (IV)
Nivolizumab (IV)
Nivolizumab (SC)
Nesvacumab (IV)
Olokizumab (IV)
Olokizumab (SC)
Ozanezumab (IV)
Patrelizumab (IV)
Pembrolizumab (IV)
Ralpancizumab (IV)
Ralpancizumab (SC)
Raxibacumab (IV)
Ricankizumab (IV)
Secukinumab (IV)
Siltuximab (IV)
Tefibazumab (IV)
Tezepelumab (IV)
Ustekinumab (IV)
Concentration (µg/mL)
Time (hours)

Figure 4.

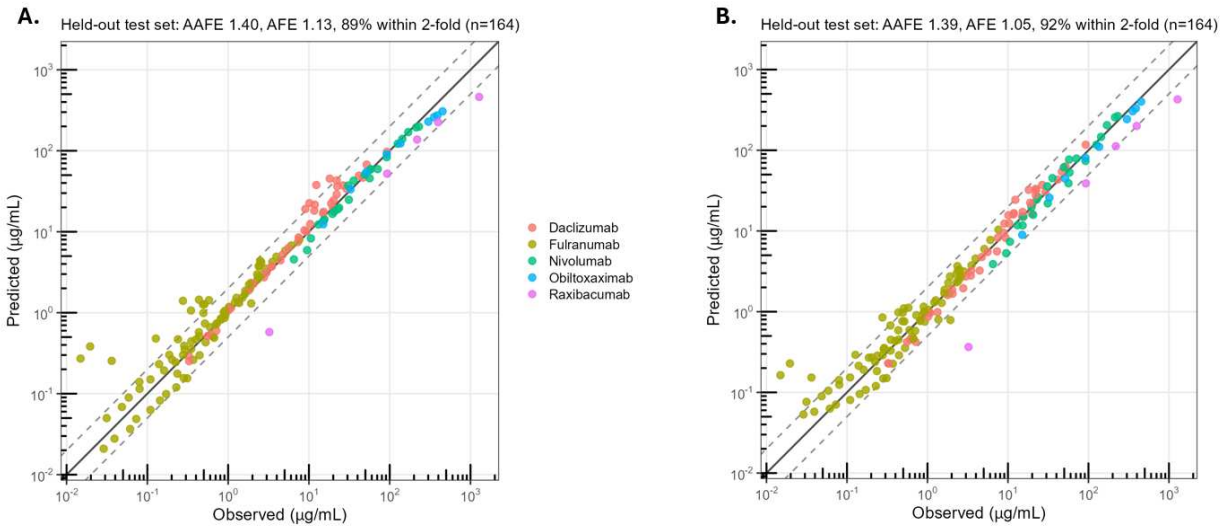

A.
Held-out test set: AAFE 1.40, AFE 1.13, 89% within 2-fold (n=164)
Predicted (µg/mL)
Observed (µg/mL)
Daclizumab
Fulranumab
Nivolumab
Obiltoxaximab
Raxibacumab
B.
Held-out test set: AAFE 1.39, AFE 1.05, 92% within 2-fold (n=164)
Predicted (µg/mL)
Observed (µg/mL)

Table 1. Summary of published clinical datasets used to develop and evaluate the proposed NODE-based PK framework. The dataset comprises 36 monoclonal antibodies, of which 21 were approved and 15 investigational at the time of the source publication. Thirty-one antibodies formed the training set; five (daclizumab, fulranumab, nivolumab, obiltoxaximab and raxibacumab) were withheld at the antibody level as an independent test set and contributed nothing to parameter estimation. Trastuzumab is not part of this dataset.

Name	Status	Analysis set	Reference
Adalimumab	Approved	Training	[22]
Belimumab	Approved	Training	[33]
Benralizumab	Approved	Training	[54]
Canakinumab	Approved	Training	[29]
Daclizumab	Approved	Test	[35]
Enokizumab	Investigational	Training	[26]
Fulranumab	Investigational	Test	[46]
Gevokizumab	Approved	Training	[28]
Guselkumab	Approved	Training	[40]
Mepolizumab	Approved	Training	[27]
Olokizumab	Investigational	Training	[32]
Ralpancizumab	Investigational	Training	[42]
Risankizumab	Approved	Training	[50, 60]
Secukinumab	Approved	Training	[48]
Tezepelumab	Approved	Training	[47]
Cemiplimab	Approved	Training	[51]
Cetrelimab	Investigational	Training	[53]
Crenezumab	Investigational	Training	[49]
Enavatuzumab	Investigational	Training	[44]
Farletuzumab	Investigational	Training	[34]
Gedivumab	Investigational	Training	[13]
Infliximab	Approved	Training	[41]
Ipilimumab	Approved	Training	[31]
Lesofavumab	Investigational	Training	[43]
Lexatumumab	Investigational	Training	[25]
Nesvacumab	Investigational	Training	[38]
Nivolumab	Approved	Test	[45]
Obiltoxaximab	Approved	Test	[37]
Ozanezumab	Investigational	Training	[13]
Pateclizumab	Investigational	Training	[30]
Pembrolizumab	Approved	Training	[39]
Raxibacumab	Approved	Test	[52]
Reslizumab	Approved	Training	[36]
Siltuximab	Approved	Training	[24]
Tefibazumab	Investigational	Training	[23]
Ublituximab	Approved	Training	[61]

Table 2. Final population parameter estimates for the NODE-2CMT and NODE-mPBPK models, estimated from the 31-antibody training set (128 dose-route profiles, 1,259 observations).

Parameter	Description	NODE-2CMT Estimate (RSE %)	NODE-mPBPK Estimate (RSE %)
Structural and disposition parameters			
CL	Linear clearance from the central compartment (mL h^{-1})	3.04 (8.82)	—
V_c	Central volume of distribution (mL)	3490 (5.57)	—
V_p	Peripheral volume of distribution (mL)	2560 (2.45)	—
Q	Inter-compartmental clearance (mL h^{-1})	21.2 (4.89)	—
k_a	First-order subcutaneous absorption rate (h^{-1})	0.0167 (4.61)	0.00735 (25.2)
σ_1	Vascular reflection coefficient, tight tissues	—	0.914 (1.63)
σ_2	Vascular reflection coefficient, leaky tissues	—	0.729 (2.20)
Embedded neural-network parameters[a]			
$w_{1,1}$	Input-layer weight	0.00615 (12.8)	56.4 (10.1)
$b_{1,1}$	Input-layer bias	0.0295 (33.0)	−3.15 (27.9)
$w_{2,1}$	Output-layer weight	0.316 (16.5)	0.199 (11.2)
$b_{2,1}$	Output-layer bias	0.0243 (30.5)	0.169 (40.7)
Inter-antibody variability (ω, as SD of η)			
ω_{Vc}	IIV on central volume	0.608 (6.44)	—
$\omega_{\sigma 1}$	IIV on σ_1	—	0.0934 (14.9)
$\omega_{\sigma 2}$	IIV on σ_2	—	0.168 (10.1)

ω_{ka}	IIV on subcutaneous absorption rate	—	1.12 (15.3)
$\omega_{w2,1}$	IIV on neural-network output weight	0.873 (7.01)	0.116 (6.68)

[a] *Neural-network weights and biases are latent parameters without direct biological interpretation; their values depend on the scaling of the network input and are not comparable between the two models. Larger relative standard errors for these parameters are an expected property of low-dimensional neural ODEs. The learned elimination function itself, rather than the individual weights, is characterized in Figure S3.*

Table 3. Predictive performance of the two models on the five antibodies withheld from estimation (daclizumab, fulranumab, nivolumab, obiltoxaximab, raxibacumab). AFE, average fold error; AAFE, absolute average fold error. Population parameters, random-effect variances and residual error parameters were fixed to the training-set estimates and were not re-estimated; antibody-specific random effects were obtained as empirical Bayes estimates conditional on the observed test data.

Model	**n observations**	**AFE**	**AAFE**	**Within 2-fold (%)**
NODE-2CMT	164	1.13	1.40	89
NODE-mPBPK	164	1.05	1.39	92

Estimates are population (fixed-effect) values obtained in Monolix 2024R1 by the SAEM algorithm; values in parentheses are relative standard errors (RSE %). "—" indicates a parameter that is not present in the corresponding model. In the NODE-mPBPK model, the physiological volumes and lymph flows were fixed to literature values for immunoglobulin G and are not listed. ω denotes the standard deviation of the corresponding random effect; because the estimation unit is a published dose-route profile rather than a subject, these terms represent combined between-profile variability (inter-antibody, inter-study, inter-route and inter-dose) rather than inter-antibody variability alone. Model fit statistics for the training set were:

NODE-2CMT, OFV 5,433.36, AIC 5,459.36, BIC 5,496.44; NODE-mPBPK, OFV 5,987.05, AIC 6,013.05, BIC 6,050.13, each with 13 estimated parameters. Residual error parameters (combined model) were a = 0.0365 µg/mL and b = 0.154 for NODE-2CMT and a = 0.0290 µg/mL and b = 0.164 for NODE-mPBPK.

References

1. Ryman JT, Meibohm B. Pharmacokinetics of monoclonal antibodies. CPT Pharmacometrics Syst Pharmacol. 2017;6(9):576-88. doi: 10.1002/psp4.12224.
2. Dirks NL, Meibohm B. Population pharmacokinetics of therapeutic monoclonal antibodies. Clin Pharmacokinet. 2010;49(10):633-59. doi: 10.2165/11535960-000000000-00000.
3. Keizer RJ, Huitema AD, Schellens JH, Beijnen JH. Clinical pharmacokinetics of therapeutic monoclonal antibodies. Clin Pharmacokinet. 2010;49(8):493-507. doi: 10.2165/11531280-000000000-00000.
4. Wang W, Wang EQ, Balthasar JP. Monoclonal antibody pharmacokinetics and pharmacodynamics. Clin Pharmacol Ther. 2008;84(5):548-58. doi: 10.1038/clpt.2008.170.
5. Mager DE, Jusko WJ. General pharmacokinetic model for drugs exhibiting target-mediated drug disposition. J Pharmacokinet Pharmacodyn. 2001;28(6):507-32. doi: 10.1023/a:1014414520282.

6. Mager DE, Krzyzanski W. Quasi-equilibrium pharmacokinetic model for drugs exhibiting target-mediated drug disposition. Pharm Res. 2005;22(10):1589-96. doi: 10.1007/s11095-005-6650-0.
7. Gibiansky L, Gibiansky E, Kakkar T, Ma P. Approximations of the target-mediated drug disposition model and identifiability of model parameters. J Pharmacokinet Pharmacodyn. 2008;35(5):573-91. doi: 10.1007/s10928-008-9102-8.
8. Cao Y, Balthasar JP, Jusko WJ. Second-generation minimal physiologically-based pharmacokinetic model for monoclonal antibodies. J Pharmacokinet Pharmacodyn. 2013;40(5):597-607. doi: 10.1007/s10928-013-9332-2.
9. Cao Y, Jusko WJ. Applications of minimal physiologically-based pharmacokinetic models. J Pharmacokinet Pharmacodyn. 2012;39(6):711-23. doi: 10.1007/s10928-012-9280-2.
10. Cao Y, Jusko WJ. Incorporating target-mediated drug disposition in a minimal physiologically-based pharmacokinetic model for monoclonal antibodies. J Pharmacokinet Pharmacodyn. 2014;41(4):375-87. doi: 10.1007/s10928-014-9372-2.
11. Shah DK, Betts AM. Towards a platform PBPK model to characterize the plasma and tissue disposition of monoclonal antibodies in preclinical species and human. J Pharmacokinet Pharmacodyn. 2012;39(1):67-86. doi: 10.1007/s10928-011-9232-2.
12. Glassman PM, Balthasar JP. Physiologically-based modeling of monoclonal antibody pharmacokinetics in drug discovery and development. Drug Metab Pharmacokinet. 2019;34(1):3-13. doi: 10.1016/j.dmpk.2018.11.002.
13. Kumar M, Lanke S, Yadav A, Ette M, Mager DE, Shah DK. Inter-Antibody Variability in the Clinical Pharmacokinetics of Monoclonal Antibodies Characterized Using Population Physiologically Based Pharmacokinetic Modeling. Antibodies. 2024;13(3):54.
14. Chen RT, Rubanova Y, Bettencourt J, Duvenaud DK. Neural ordinary differential equations. Advances in neural information processing systems. 2018;31.
15. Rackauckas C, Ma Y, Martensen J, Warner C, Zubov K, Supekar R, et al. Universal differential equations for scientific machine learning. arXiv preprint arXiv:200104385. 2020.
16. Hornik K, Stinchcombe M, White H. Multilayer feedforward networks are universal approximators. Neural Networks. 1989;2(5):359-66. doi: https://doi.org/10.1016/0893-6080(89)90020-8.
17. Losada IB, Terranova N. Bridging pharmacology and neural networks: A deep dive into neural ordinary differential equations. CPT Pharmacometrics Syst Pharmacol. 2024;13(8):1289-96. doi: 10.1002/psp4.13149.
18. Lu J, Deng K, Zhang X, Liu G, Guan Y. Neural-ODE for pharmacokinetics modeling and its advantage to alternative machine learning models in predicting new dosing regimens. iScience. 2021;24(7):102804. doi: 10.1016/j.isci.2021.102804.
19. Janssen A, Leebeek FWG, Cnossen MH, Mathôt RAA. Deep compartment models: A deep learning approach for the reliable prediction of time-series data in pharmacokinetic modeling. CPT Pharmacometrics Syst Pharmacol. 2022;11(7):934-45. doi: 10.1002/psp4.12808.
20. Bräm DS, Nahum U, Schropp J, Pfister M, Koch G. Low-dimensional neural ODEs and their application in pharmacokinetics. Journal of Pharmacokinetics and Pharmacodynamics. 2024;51(2):123-40. doi: 10.1007/s10928-023-09886-4.

21. Bräm DS, Steiert B, Pfister M, Steffens B, Koch G. Low-dimensional neural ordinary differential equations accounting for inter-individual variability implemented in Monolix and NONMEM. CPT Pharmacometrics Syst Pharmacol. 2025;14(1):5-16. doi: 10.1002/psp4.13265.
22. Weisman MH, Moreland LW, Furst DE, Weinblatt ME, Keystone EC, Paulus HE, et al. Efficacy, pharmacokinetic, and safety assessment of adalimumab, a fully human anti-tumor necrosis factor-alpha monoclonal antibody, in adults with rheumatoid arthritis receiving concomitant methotrexate: a pilot study. Clin Ther. 2003;25(6):1700-21. doi: 10.1016/s0149-2918(03)80164-9.
23. Reilley S, Wenzel E, Reynolds L, Bennett B, Patti Joseph M, Hetherington S. Open-Label, Dose Escalation Study of the Safety and Pharmacokinetic Profile of Tefibazumab in Healthy Volunteers. Antimicrobial Agents and Chemotherapy. 2005;49(3):959-62. doi: 10.1128/aac.49.3.959-962.2005.
24. Puchalski T, Prabhakar U, Jiao Q, Berns B, Davis HM. Pharmacokinetic and pharmacodynamic modeling of an anti–interleukin-6 chimeric monoclonal antibody (siltuximab) in patients with metastatic renal cell carcinoma. Clinical Cancer Research. 2010;16(5):1652-61.
25. Wakelee HA, Patnaik A, Sikic BI, Mita M, Fox NL, Miceli R, et al. Phase I and pharmacokinetic study of lexatumumab (HGS-ETR2) given every 2 weeks in patients with advanced solid tumors. Ann Oncol. 2010;21(2):376-81. doi: 10.1093/annonc/mdp292.
26. Parker JM, Oh CK, LaForce C, Miller SD, Pearlman DS, Le C, et al. Safety profile and clinical activity of multiple subcutaneous doses of MEDI-528, a humanized anti-interleukin-9 monoclonal antibody, in two randomized phase 2a studies in subjects with asthma. BMC Pulm Med. 2011;11:14. doi: 10.1186/1471-2466-11-14.
27. Smith DA, Minthorn EA, Beerahee M. Pharmacokinetics and pharmacodynamics of mepolizumab, an anti-interleukin-5 monoclonal antibody. Clinical pharmacokinetics. 2011;50(4):215-27.
28. Cavelti-Weder C, Babians-Brunner A, Keller C, Stahel MA, Kurz-Levin M, Zayed H, et al. Effects of gevokizumab on glycemia and inflammatory markers in type 2 diabetes. Diabetes care. 2012;35(8):1654-62.
29. Chakraborty A, Tannenbaum S, Rordorf C, Lowe PJ, Floch D, Gram H, Roy S. Pharmacokinetic and pharmacodynamic properties of canakinumab, a human anti-interleukin-1β monoclonal antibody. Clin Pharmacokinet. 2012;51(6):e1-18. doi: 10.2165/11599820-000000000-00000.
30. Emu B, Luca D, Offutt C, Grogan JL, Rojkovich B, Williams MB, et al. Safety, pharmacokinetics, and biologic activity of pateclizumab, a novel monoclonal antibody targeting lymphotoxin α: results of a phase I randomized, placebo-controlled trial. Arthritis Res Ther. 2012;14(1):R6. doi: 10.1186/ar3554.
31. Feng Y, Masson E, Dai D, Parker SM, Berman D, Roy A. Model-based clinical pharmacology profiling of ipilimumab in patients with advanced melanoma. British journal of clinical pharmacology. 2014;78(1):106-17.
32. Kretsos K, Golor G, Jullion A, Hickling M, McCabe S, Shaw S, et al. Safety and pharmacokinetics of olokizumab, an anti-IL-6 monoclonal antibody, administered to

healthy male volunteers: A randomized phase I study. Clinical Pharmacology in Drug Development. 2014;3(5):388-95.
33. Shida Y, Takahashi N, Sakamoto T, Ino H, Endo A, Hirama T. The pharmacokinetics and safety profiles of belimumab after single subcutaneous and intravenous doses in healthy Japanese volunteers. J Clin Pharm Ther. 2014;39(1):97-101. doi: 10.1111/jcpt.12101.
34. Sasaki Y, Miwa K, Yamashita K, Sunakawa Y, Shimada K, Ishida H, et al. A phase I study of farletuzumab, a humanized anti-folate receptor α monoclonal antibody, in patients with solid tumors. Investigational new drugs. 2015;33(2):332-40.
35. Diao L, Hang Y, Othman AA, Nestorov I, Tran JQ. Population pharmacokinetics of daclizumab high-yield process in healthy volunteers and subjects with multiple sclerosis: analysis of phase I–III clinical trials. Clinical pharmacokinetics. 2016;55(8):943-55.
36. FDA. Reslizumab NDA Clinical Pharmacology and Biopharmaceutics Review. In: Research CfDEa, editor.2016.
37. Nagy CF, Leach TS, Hoffman JH, Czech A, Carpenter SE, Guttendorf R. Pharmacokinetics and Tolerability of Obiltoxaximab: A Report of 5 Healthy Volunteer Studies. Clin Ther. 2016;38(9):2083-97.e7. doi: 10.1016/j.clinthera.2016.07.170.
38. Papadopoulos KP, Kelley RK, Tolcher AW, Razak AR, Van Loon K, Patnaik A, et al. A Phase I First-in-Human Study of Nesvacumab (REGN910), a Fully Human Anti-Angiopoietin-2 (Ang2) Monoclonal Antibody, in Patients with Advanced Solid Tumors. Clin Cancer Res. 2016;22(6):1348-55. doi: 10.1158/1078-0432.Ccr-15-1221.
39. Shimizu T, Seto T, Hirai F, Takenoyama M, Nosaki K, Tsurutani J, et al. Phase 1 study of pembrolizumab (MK-3475; anti-PD-1 monoclonal antibody) in Japanese patients with advanced solid tumors. Investigational new drugs. 2016;34(3):347-54.
40. Zhuang Y, Calderon C, Marciniak SJ, Bouman-Thio E, Szapary P, Yang T-Y, et al. First-in-human study to assess guselkumab (anti-IL-23 mAb) pharmacokinetics/safety in healthy subjects and patients with moderate-to-severe psoriasis. European Journal of Clinical Pharmacology. 2016;72(11):1303-10. doi: 10.1007/s00228-016-2110-5.
41. Ehrenpreis ED. Pharmacokinetic effects of antidrug antibodies occurring in healthy subjects after a single dose of intravenous infliximab. Drugs in R&D. 2017;17(4):607-13.
42. Levisetti M, Joh T, Wan H, Liang H, Forgues P, Gumbiner B, Garzone PD. A Phase I Randomized Study of a Specifically Engineered, pH-Sensitive PCSK9 Inhibitor RN317 (PF-05335810) in Hypercholesterolemic Subjects on Statin Therapy. Clin Transl Sci. 2017;10(1):3-11. doi: 10.1111/cts.12430.
43. Lim JJ, Derby MA, Zhang Y, Deng R, Larouche R, Anderson M, et al. A Phase 1, Randomized, Double-Blind, Placebo-Controlled, Single-Ascending-Dose Study To Investigate the Safety, Tolerability, and Pharmacokinetics of an Anti-Influenza B Virus Monoclonal Antibody, MHAB5553A, in Healthy Volunteers. Antimicrob Agents Chemother. 2017;61(8). doi: 10.1128/aac.00279-17.
44. Lam ET, Eckhardt SG, Messersmith W, Jimeno A, O'Bryant CL, Ramanathan RK, et al. Phase I Study of Enavatuzumab, a First-in-Class Humanized Monoclonal Antibody Targeting the TWEAK Receptor, in Patients with Advanced Solid Tumors. Mol Cancer Ther. 2018;17(1):215-21. doi: 10.1158/1535-7163.Mct-17-0330.

45. Lee KW, Lee DH, Kang JH, Park JO, Kim SH, Hong YS, et al. Phase I Pharmacokinetic Study of Nivolumab in Korean Patients with Advanced Solid Tumors. Oncologist. 2018;23(2):155-e17. doi: 10.1634/theoncologist.2017-0528.
46. Kelly KM, Sanga P, Zaki N, Wang S, Haeussler J, Louie J, Thipphawong J. Safety and efficacy of fulranumab in osteoarthritis of the hip and knee: results from four early terminated phase III randomized studies. Curr Med Res Opin. 2019;35(12):2117-27. doi: 10.1080/03007995.2019.1653068.
47. Parnes JR, Sullivan JT, Chen L, Dias C. Pharmacokinetics, safety, and tolerability of tezepelumab (AMG 157) in healthy and atopic dermatitis adult subjects. Clinical Pharmacology & Therapeutics. 2019;106(2):441-9.
48. Bruin G, Hockey HUP, La Stella P, Sigurgeirsson B, Fu R, Patekar M, et al. Comparison of pharmacokinetics, safety and tolerability of secukinumab administered subcutaneously using different delivery systems in healthy volunteers and in psoriasis patients. British journal of clinical pharmacology. 2020;86(2):338-51.
49. Guthrie H, Honig LS, Lin H, Sink KM, Blondeau K, Quartino A, et al. Safety, Tolerability, and Pharmacokinetics of Crenezumab in Patients with Mild-to-Moderate Alzheimer's Disease Treated with Escalating Doses for up to 133 Weeks. J Alzheimers Dis. 2020;76(3):967-79. doi: 10.3233/jad-200134.
50. Pang Y, Khatri A, Suleiman AA, Othman AA. Clinical Pharmacokinetics and Pharmacodynamics of Risankizumab in Psoriasis Patients. Clin Pharmacokinet. 2020;59(3):311-26. doi: 10.1007/s40262-019-00842-5.
51. Papadopoulos KP, Johnson ML, Lockhart AC, Moore K, Falchook GS, Formenti SC, et al. First-In-Human Study of Cemiplimab Alone or In Combination with Radiotherapy and/or Low-dose Cyclophosphamide in Patients with Advanced Malignancies. Clin Cancer Res. 2020;26(5):1025-33. doi: 10.1158/1078-0432.Ccr-19-2609.
52. Skoura N, Wang-Jairaj J, Della Pasqua O, Chandrasekaran V, Billiard J, Yeakey A, et al. Effect of raxibacumab on immunogenicity of Anthrax Vaccine Adsorbed: a phase 4, open-label, parallel-group, randomised non-inferiority study. The Lancet Infectious Diseases. 2020;20(8):983-91.
53. Felip E, Moreno V, Morgensztern D, Curigliano G, Rutkowski P, Trigo JM, et al. First-in-human, open-label, phase 1/2 study of the monoclonal antibody programmed cell death protein-1 (PD-1) inhibitor cetrelimab (JNJ-63723283) in patients with advanced cancers. Cancer Chemother Pharmacol. 2022;89(4):499-514. doi: 10.1007/s00280-022-04414-6.
54. Martin UJ, Fuhr R, Forte P, Barker P, Axley MJ, Aurivillius M, et al. Comparison of autoinjector with accessorized prefilled syringe for benralizumab pharmacokinetic exposure: AMES trial results. Journal of Asthma. 2021;58(1):93-101.
55. Rohatgi A: WebPlotDigitizer. https://automeris.io (5.2). Accessed.
56. Yan X, Mager DE, Krzyzanski W. Selection between Michaelis-Menten and target-mediated drug disposition pharmacokinetic models. J Pharmacokinet Pharmacodyn. 2010;37(1):25-47. doi: 10.1007/s10928-009-9142-8.
57. Simulations Plus LD. Monolix 2024R1. 2024.
58. Zhang T, Androulakis IP, Bonate P, Cheng L, Helikar T, Parikh J, et al. Two heads are better than one: current landscape of integrating QSP and machine learning : An ISoP QSP SIG white paper by the working group on the integration of quantitative systems

pharmacology and machine learning. J Pharmacokinet Pharmacodyn. 2022;49(1):5-18. doi: 10.1007/s10928-022-09805-z.
59. Pore S, Roy K. Machine Learning (ML)-driven quantitative structure-pharmacokinetic relationship (QSPKR) modeling of the tissue-to-plasma partition coefficient (Kp) of drugs across different tissues. Artificial Intelligence Chemistry. 2025;3(2):100093. doi: https://doi.org/10.1016/j.aichem.2025.100093.
60. Khatri A, Eckert D, Oberoi R, Suleiman A, Pang Y, Cheng L, Othman AA. Pharmacokinetics of Risankizumab in Asian Healthy Subjects and Patients With Moderate to Severe Plaque Psoriasis, Generalized Pustular Psoriasis, and Erythrodermic Psoriasis. J Clin Pharmacol. 2019;59(12):1656-68. doi: 10.1002/jcph.1473.
61. Sawas A, Farber CM, Schreeder MT, Khalil MY, Mahadevan D, Deng C, et al. A phase 1/2 trial of ublituximab, a novel anti-CD20 monoclonal antibody, in patients with B-cell non-Hodgkin lymphoma or chronic lymphocytic leukaemia previously exposed to rituximab. British Journal of Haematology. 2017;177(2):243-53. doi: https://doi.org/10.1111/bjh.14534.

Supplementary Files

This is a list of supplementary files associated with this preprint. Click to download.

- SupplementaryAppendixv2.docx